Pharm Res (2014) 31:2297–2311
DOI 10.1007/s11095-014-1325-3

RESEARCH PAPER

Prediction of Passive Drug Permeability Across the Blood-Retinal Barrier

Aapo Tervonen • Iina Vainio • Soile Nymark • Jari Hyttinen

Received: 25 October 2013 / Accepted: 28 January 2014 / Published online: 13 March 2014

ABSTRACT

Purpose The purpose of this study is to develop a computational model of the physical barrier function of the outer blood-retinal barrier (BRB), which is vital for normal retinal function. To our best knowledge no comprehensive models of BRB has been reported.

Methods The model construction is based on the three-layered structure of the BRB: retinal pigment epithelium (RPE), Bruch's membrane and choriocapillaris endothelium. Their permeabilities were calculated based on the physical theories and experimental material and permeability studies in the literature, which were used to describe diffusional hindrance in specific environments.

Results Our compartmental BRB model predicts permeabilities with magnitudes similar to the experimental values in the literature. However, due to the small number and varying experimental conditions there is a large variability in the available experimental data, rendering validation of the model difficult. The model suggests that the paracellular pathway of the RPE largely defines the total BRB permeability.

Conclusions Our model is the first BRB model of its level and combines the present knowledge of the BRB barrier function. Furthermore, the model forms a platform for the future model development to be used for the design of new drugs and drug administration systems.

KEY WORDS blood-retinal barrier · permeability · structure-based model · compartmental model · lipophilicity

A. Tervonen (✉) • I. Vainio • S. Nymark • J. Hyttinen
BioMediTech, Tampere University of Technology, Tampere, Finland
e-mail: aapo.tervonen@tut.fi

A. Tervonen • I. Vainio • S. Nymark • J. Hyttinen
Department of Electronics and Communications Engineering
Tampere University of Technology, Box 692, Tampere 33101, Finland

ABBREVIATIONS AND NOTATION

Å	Angstrom (1 Å = 1×10^{-10} m)
AMD	Age-related macular degeneration
BRB	Outer blood-retinal barrier
BrM	Bruch's membrane
CE	Choriocapillaris endothelium
Da	Dalton (1 Da = 1.66×10^{-27} kg)
D_0	free diffusion coefficient ($m^2\ s^{-1}$)
$D_{eff,m}$	Effective diffusion coefficient within the matrix *m* ($m^2\ s^{-1}$)
D_{lat}	Lateral diffusion coefficient within the membrane ($m^2\ s^{-1}$)
D_{ICL}	Effective diffusion coefficient within ICL ($m^2\ s^{-1}$)
d_{ICL}	ICL thickness (m)
D_{OCL}	Effective diffusion coefficient within OCL ($m^2\ s^{-1}$)
d_{OCL}	OCL thickness (m)
D_m	Diffusion coefficient within the matrix *m* ($m^2\ s^{-1}$)
$d_{lat,i}$	Diffusion distance of *i*th part of the lateral diffusion pathway ($m\ s^{-1}$)
d_{RPE}	RPE cell flat-to-flat diameter (m)
d_{TJp}	TJ pore separation (m)
f	Adjusted fiber volume fraction
F_m	Hydrodynamic interactions in matrix *m*
h_{fen}	Fenestration height (m)
h_{LS}	Lateral space height (m)
$H_p(\lambda_p)$	Pore hindrance factor
h_{pore}	Pore height (m)
h_{RPE}	RPE cell height (m)
$H_s(\lambda_s)$	Slit hindrance factor
h_{slit}	Slit height (m)
h_{TJ}	TJ region height (m)
h_{TJs}	TJ strand height (m)
h_{TJss}	TJ strand separation (m)
ICL	Inner collagenous layer
K_{mem}	Membrane distribution coefficient
k_B	Boltzmann's constant ($1.38 \times 10^{-23}\ J\ K^{-1}$)
K_D	Octanol-water distribution coefficient
l_{cb}	Cell boundary length per unit area ($m\ m^{-2}$)
M_s	Solute's molecular mass (Da)
m	Membrane size selectivity (Da^{-1})
n_{TJs}	TJ strand number
OCL	Outer collagenous layer
P_{BRB}	BRB permeability coefficient ($m\ s^{-1}$)
P_{BrM}	BrM permeability coefficient ($m\ s^{-1}$)
P_{cyt}	Cytoplasm permeability coefficient ($m\ s^{-1}$)

P_{CE}	CE permeability coefficient (m s^{-1})
P_{ICL}	ICL permeability coefficient (m s^{-1})
P_{lat}	Lateral diffusion transcellular permeability coefficient (m s^{-1})
P_{OCL}	OCL permeability coefficient (m s^{-1})
$P_{lat,i}$	Permeability coefficient of *i*th part of the lateral diffusion pathway (m s^{-1})
P_{LS}	Lateral space permeability coefficient (m s^{-1})
P_{mem}	Membrane permeability coefficient (m s^{-1})
P^{0}_{mem}	Membrane permeability coefficient of a theoretical infinitely small molecule (m s^{-1})
P_{para}	Paracellular permeability coefficient (m s^{-1})
P_{pore}	Pore permeability coefficient (m s^{-1})
P_{RPE}	RPE permeability coefficient (m s^{-1})
P_{slit}	Slit permeability coefficient (m s^{-1})
P_{TJ}	TJ permeability coefficient (m s^{-1})
P_{TJl}	TJ leak pathway permeability coefficient (m s^{-1})
P_{TJp}	TJ pore pathway permeability coefficient (m s^{-1})
P_{TJs}	TJ strand permeability coefficient (m s^{-1})
P_{TJss}	Permeability coefficient of the space between TJ strands (m s^{-1})
P_{tr}	Transverse transcellular permeability coefficient (m s^{-1})
P_{trans}	Transcellular permeability coefficient (m s^{-1})
RPE	Retinal pigment epithelium
r_{CF}	Collagen fibril radius (m)
r_{dia}	Diaphragm pore radius (m)
r_f	Fiber radius (m)
r_{PG}	Proteoglycan radius (m)
r_{pore}	Pore radius (m)
r^{*}_{RPE}	Average RPE cell radius (m)
r_s	Solute molecule's radius (m)
r_{TJp}	TJ pore radius (m)
S_m	Steric interactions in matrix *m*
T	Absolute temperature (K)
TJ	Tight junctions
τ_{RPE}	RPE lateral space tortuosity
W_{LS}	Lateral space half-width (m)
W_{slit}	Slit half-width (m)
α_{leak}	TJ leak parameter
$\varepsilon_{lat,i}$	Hindrance factor of *i*th part of the lateral diffusion pathway (m s^{-1})
ε_{LS}	Relative surface area of the lateral space
ε_{pore}	Relative surface area of the pores
ε_{slit}	Relative surface area of the slit
ε_{TJp}	Relative surface area of the TJ pores
$\phi_{CF,ICL}$	Collagen volume fraction in ICL
$\phi_{CF,OCL}$	Collagen volume fraction in OCL
Φ_m	Partition coefficient between the matrix *m* and solvent
ϕ_f	Fiber volume fraction
$\phi_{PG,ICL}$	Proteoglycan volume fraction in ICL
$\phi_{PG,OCL}$	Proteoglycan volume fraction in OCL
ε_{dia}	Relative surface area of the diaphragm pores
η	Dynamic viscosity (Pa s)

INTRODUCTION

An important part of the blood-ocular barrier is the outer blood-retinal barrier (BRB), which is a three-layered structure in the eye, between the retina and choroid. It has many important roles in normal retinal function. It forms the barrier between the systemic blood circulation and the delicate retinal environment. In addition, the BRB is the primary location for many retinal diseases, most notably age-related macular degeneration (AMD), which causes visual impairment or even loss of vision (1,2). In this article, we describe a computational, structure-based model of passive diffusion across the BRB for the prediction of molecular permeability.

The BRB forms a challenge for drug administration against the retinal diseases because it retards the passive drug permeation from the systemic circulation. Moreover, also the anterior administration pathways that avoid the BRB, such as eye drops or intraocular injections, have their disadvantages (3). Nowadays, an emerging administration pathway is through the sclera, which is more permeable than the cornea and closer to the retina. Transscleral drug delivery is more targeted than systemic administration or eye drops, and less risky than intraocular injections. However, with this type of administration as well the BRB forms a barrier against the drug permeation (3). In order to improve transscleral drug delivery systems, detailed model of the BRB barrier properties is well warranted.

The BRB consists of three components: retinal pigment epithelium (RPE), Bruch's membrane (BrM) and choriocapillaris endothelium (CE). RPE is formed by a monolayer of pigment RPE cells, and it is the tightest component, largely because of the tight junctions (TJ) between the cells (2). RPE lies on the BrM, which is a thin extracellular matrix layer and forms a passive barrier against the diffusion (4). CE is a fenestrated endothelium and it is the most permeable component in the BRB (2). Permeability of a molecule through these layers is determined by its physicochemical properties, such as size and lipophilicity (5), which further define interactions between the molecule and the BRB components.

Computational models based on the properties of the diffusing molecule and the tissue material properties and structure as well as physical laws may provide an easy and inexpensive method to better understand the components and behavior of BRB barrier properties. In addition, a validated model of BRB could be used to design and validate *in vitro* BRB models for drug development and delivery systems. At the moment, there are no such models available. There are only few computational diffusion models that include the BRB, most of which are pharmacokinetic models (6–8) with phenomenological characteristics. Many of the existing models describe the BRB with a single permeability coefficient (6,7,9) and one model uses three coefficients for different molecule types (8). The model by Haghjou *et al.* (10) took a step further by relating the physicochemical properties of the molecule to the permeability across the retina, choroid and sclera. In all of these models, the BRB plays

only a small role, because all the layers of the eye (6–8) or even the whole eye (9,10) are included in the models. However, for some other tissues there are more detailed and structure-based models of other anatomical barriers, such as cornea (11,12) and skin (13), which are based on the properties of both the molecule and the tissue material and structure of the barrier. This kind of models can connect the permeability of a molecule to its interactions with the barrier and provide information about the actual diffusion pathway and rate-limiting components.

In the present study, we introduce a structure-based, compartmental computational model based on the physical laws of passive diffusion across human BRB. To our knowledge, such model has not been published earlier. Our model, reflecting the corneal model of Edwards & Prausnitz (12), aims to relate the properties of the molecule, such as the lipophilicity and radius, to the permeability of the material and to the tissue diffusion pathways. Also, we introduce a TJ model structure for epithelial model. We gather the present knowledge regarding the structural components of the BRB by providing the structural parameters of the model. These were extracted either directly from the literature or were approximated based on available data. Furthermore, we provide parameter sensitivity analysis indicating the importance of given parameters in BRB modeling. In addition, we summarize and discuss the characteristics of the presently available experimental data of BRB permeability. Altogether, the model combines our present knowledge of the BRB passive diffusion-based barrier properties.

METHODS

The main function of the model is to produce permeability coefficients for each component and pathway of the diffusion across the BRB based on the given molecular property inputs. The RPE and BrM models are largely based on the computational framework established for corneal diffusion model by Edwards & Prausnitz (11,12). The two barriers are similar in many ways: they both consist of an epithelium, an extracellular matrix layer and an endothelium. There are some major differences, such as the thickness of the extracellular matrix layer and the number of the cell layers (2,12). The main differences between their and our models result from these tissue characteristics as well as from some refined equations used in the present model. Equations used or based on the equations used by them are 2, 4, 11–13, 17, 20, 21 and 24. All the calculations were performed with MATLAB (version R2012a, The MathWorks, Inc., Natick, Massachusetts, United States).

The Diffusion Pathways and the Geometry of the Model

The three components of the BRB and the way they are divided into the main pathways and permeability subcomponents are shown in Fig. 1. RPE is divided into two main pathways: the paracellular pathway between the cells and transcellular pathway through the cells. The latter is further divided into two: transverse diffusion across the cell membranes and cytoplasm and lateral diffusion along the cell membrane. The geometrical basis of the compartmental RPE model is presented in Fig. 2. The hexagonal RPE cells are presented with perfect hexagonal cylinders, ignoring the more detailed surface characteristics (Fig. 2a). Small space is left between the neighboring cells to represent the lateral space, which is closed near the apical membrane by TJs (Fig. 2c). The web-like structure of the TJs (14) is modeled with parallel strands that encircle the cells (Fig 2b). Two pathways are modeled for the TJs: small molecules can pass through small pores formed between so-called 10-nm particles in the strands and larger molecules through the breaks in the

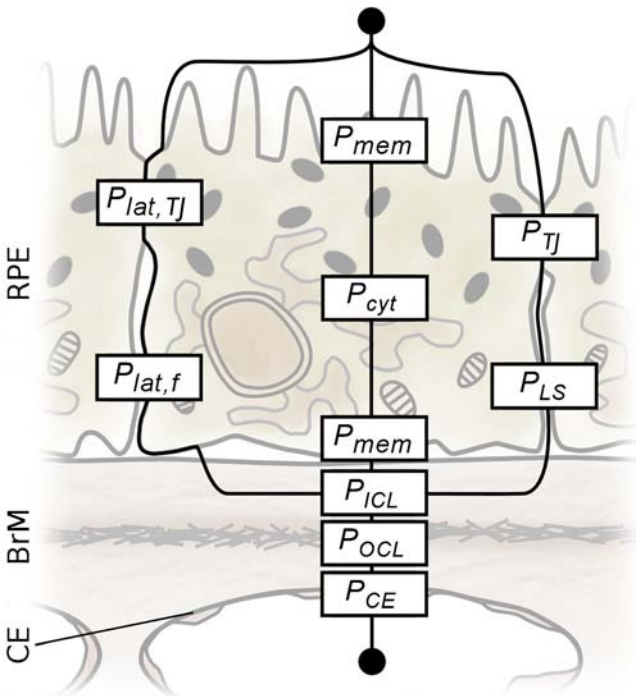

Fig. 1 The pathways and their subcomponents across the BRB (*RPE* retinal pigment epithelium, *BrM* Bruch's membrane, *CE* Choriocapillaris endothelium, $P_{lat,TJ}$ permeability of the lateral pathway TJ component, $P_{lat,f}$ permeability of the lateral pathway free component, P_{mem} membrane permeability, P_{cyt} cytosol permeability, P_{TJ} TJ permeability, P_{LS} lateral space permeability, P_{ICL} inner collagenous layer permeability, P_{OCL} outer collagenous layer permeability, P_{CE} choriocapillaris endothelium permeability).

strands, caused by their dynamic nature (14). A similar dual pathway model was introduced by Guo *et al.* (15) as they determined the structure of the TJs in renal tubules.

BrM is modeled with two collagenous layers—the inner (ICL) and outer collagenous layers (OCL)—which form the bulk of it. Both layers are represented with randomly oriented collagen fibrils and ground substance consisting of proteoglycans, which quite well corresponds to the real BrM structure (4). The main differences between the layers are that ICL is more tightly interwoven and has twice the thickness of the OCL (16).

Because the fenestrations are permeable to even macromolecules, other diffusion pathways are ignored in the CE model. The fenestrations have diaphragms spanning over them, consisting of eight radial fibrils that leave triangular pores between them (Fig. 2d) (17).

Diffusion Across the Retinal Pigment Epithelium

In the present work, RPE is modeled by connecting the paracellular and transcellular diffusion pathways in parallel, as described by equation

$$P_{RPE} = P_{para} + P_{trans}, \tag{1}$$

where P_{RPE}, P_{para} and P_{trans} are the permeability coefficients (unit m s^{-1}) of the RPE, paracellular pathway and transcellular pathway, respectively. The main assumption in the model is that a solute cannot change pathway when permeating across the RPE.

Paracellular Pathway

The paracellular pathway is modeled with the lateral space and TJs connected in series. A so-called slit model (18) is used to model the lateral space. The permeability coefficient for a solute molecule with a radius of r_s (m) in a slit with a width of $2W_{slit}$ (m) is given as

$$P_{slit} = \frac{\varepsilon_{slit} D_0 H_s(r_s/W_{slit})}{h_{slit}}, \tag{2}$$

where ε_{slit} is the relative surface area of the slit, D_0 is the solute's free diffusion coefficient (m^2 s^{-1}), H_s is the slit hindrance factor as a function of r_s/W_{slit} and h_{slit} is the slit height (m). The slit hindrance factor H_s includes the effects of solute partitioning into the slit as well as the hydrodynamic and steric interactions with its walls. Hydrodynamic interactions are interactions between the solute and the wall mediated by the solvent (19). A function for H_s was determined by Dechadilok & Deen (20) as

$$H_s(\lambda_s) = 1 + \frac{9}{16}\lambda_s \ln\lambda_s - 1.19358\lambda_s + 0.4285\lambda_s^3 - 0.3192\lambda_s^4 + 0.08428\lambda_s^5, \tag{3}$$

where $\lambda_s = r_s/W_{slit}$. The lateral space height is calculated as $h_{LS} = \tau_{RPE}(h_{RPE} - h_{TJ})$ (m), where τ_{RPE} is the lateral space

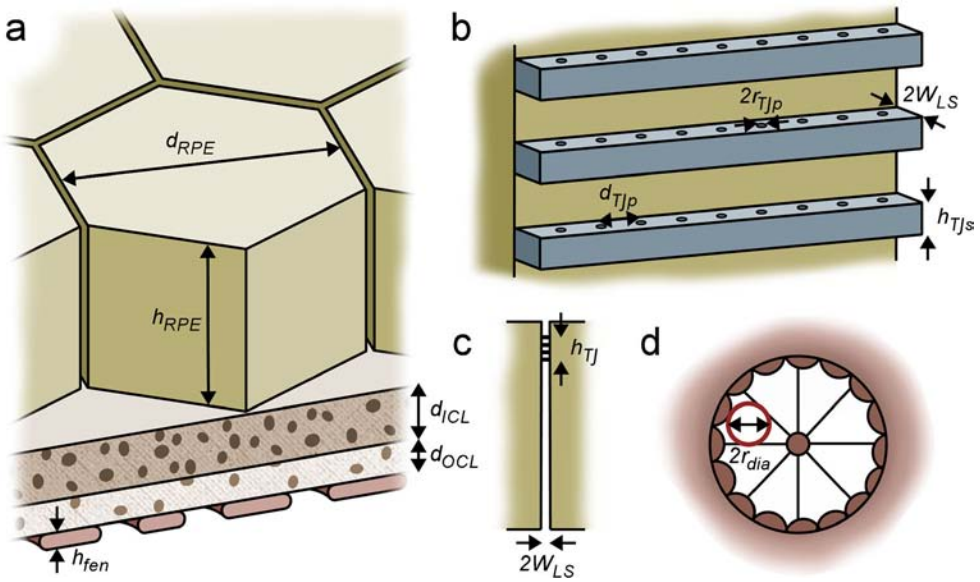

Fig. 2 The geometrical idea of the model. (**a**) The three layers of BRB: retinal pigment epithelium RPE, Bruch's membrane and choriocapillaris endothelium (d_{RPE} RPE flat-to-flat diameter, h_{RPE} RPE cell height, d_{ICL} ICL thickness, d_{OCL} OCL thickness, h_{fen} fenestration height). (**b**) The geometrical illustration of the TJ model, showing the strands and pores (r_{TJp} TJ pore radius, W_{LS} lateral space half-width, d_{TJp} TJ pore separation, h_{TJs} TJ strand height). (**c**) The lateral space between the RPE cells, closed off by the TJs on the apical end (h_{TJ} TJ region height). (**d**) A CE fenestration showing the radial fibrils and the circular pore used to model the openings (r_{fen} fenestration pore radius).

tortuosity, h_{RPE} and h_{TJ} are the RPE cell height (m) and TJ region height (m), respectively. For lateral space, the relative surface area can be calculated as

$$\varepsilon_{LS} = 2W_{LS}l_{cb} = 2W_{LS}\left[\left(\frac{2}{\sqrt{3}d_{RPE}^2}\right)\left(\frac{12}{\sqrt{3}}\frac{d_{RPE}}{2}\right)\frac{1}{2}\right], \quad (4)$$

where W_{LS} is the lateral space half-width (m), l_{cb} is the cell boundary length per unit area (m m^{-2}) and d_{RPE} is the hexagonal RPE cell flat-to-flat diameter (m). The part in square brackets is the cell density times the circumference of one cell divided by two to encounter the fact that cell boundaries are calculated twice.

The TJ pore pathway is modeled by connecting n_{TJs} number of parallel strands and $(n_{TJs}-1)$ number of spaces between the strands in series. Each TJ strand is modeled as a barrier having equally spaced pores through it, and the strand permeability is calculated using a so-called pore model (18). The permeability of a solute through pores with a radius of r_{pore} (m) is given by

$$P_{pore} = \frac{\varepsilon_{pore}D_0H_p(r_s/r_{pore})}{h_{pore}}, \quad (5)$$

where ε_{pore} is the relative surface area of the pores, H_p is the pore hindrance factor as a function of r_s/r_{pore} and h_{pore} is the pore height (m). H_p is analogous to the slit hindrance factor, and its function was determined by Dechadilok & Deen (20) as

$$H_p(\lambda_p) = 1+\frac{9}{8}\lambda_p\ln\lambda_p - 1.56034\lambda_p + 0.528155\lambda_p^2 + 1.91521\lambda_p^3 - 2.81903\lambda_p^4 + 0.270788\lambda_p^5 + 1.10115\lambda_p^6 - 0.435933\lambda_p^7, \quad (6)$$

where $\lambda_p = r_s/r_{pore}$. The relative surface area of the TJ pores can be calculated as

$$\varepsilon_{TJp} = \pi r_{TJp}^2\frac{l_{cb}}{d_{TJp}}, \quad (7)$$

where r_{TJp} is the TJ pore radius (m), l_{cb} is calculated as shown in Eq. 4 and d_{TJp} is the TJ pore separation (m). The spaces between strands are modeled with the slit model (Eq. 2), using the same values for ε_{slit} and W_{slit} as with the lateral space but with height $h_{TJss} = (h_{TJ} - n_{TJs}\,h_{TJs})/(n_{TJs}-1)$, where h_{TJs} (m) is the TJ strand height. The total TJ pore pathway permeability is calculated as

$$P_{TJp} = \left(\frac{n_{TJs}}{P_{TJs}} + \frac{n_{TJs}-1}{P_{TJss}}\right)^{-1}, \quad (8)$$

where P_{TJs} is the TJ strand permeability and P_{TJss} is the permeability of the space between the strands.

The TJ leak pathway model does not take into account the TJ strand structure, but this pathway is modeled using the slit model (Eq. 2) and multiplying it with parameter α_{leak}, which describes the amount of strand breaks and the effect of the TJ network structure on the leak pathway permeability. The slit height used in the model is h_{TJ}.

The total TJ permeability can be calculated from equation

$$P_{TJ} = P_{TJp} + P_{TJl}, \quad (9)$$

where P_{TJl} is the TJ leak pathway permeability, and the total paracellular permeability is given by equation

$$P_{para} = \left(\frac{1}{P_{LS}} + \frac{1}{P_{TJ}}\right)^{-1}, \quad (10)$$

where P_{LS} is the lateral space permeability.

Transcellular Pathway

In the transcellular pathway, the transverse and lateral diffusion pathways are connected in parallel, similarly to Edwards & Prausnitz (12). The transverse pathway consists of the solute 1) permeating the basolateral cell membrane, 2) diffusing across the cell cytoplasm and 3) permeating the apical cell membrane. The lateral diffusion pathway consists of the solute 1) partitioning into the basolateral cell membrane, 2) diffusing within the cell membrane around the cytoplasm and 3) partitioning out from the membrane in the apical side.

The cell membrane permeation model by Edwards & Prausnitz utilized data by Lieb & Stein (21). The present model uses the same data, but the equation parameters (m, A and B) are parameterized based on the molecular mass rather than van der Waals volume used by Lieb & Stein. The cell membrane permeability is given as

$$P_{mem} = P_{mem}^0 10^{-mM_s}, \quad (11)$$

where P^0_{mem} is the membrane permeability of a theoretical, infinitely small molecule, m is the membrane size selectivity (0.03034 Da^{-1}) and M_s is the solute's molecular mass (Da). P^0_{mem} as a function of lipophilicity is given by equation

$$\log P_{mem}^0 = A\log K_D + B, \quad (12)$$

where A and B are fitted parameters with values 1.355 and −3.655, respectively, and K_D is the solute molecule's octanol/water distribution coefficient at pH 7.4. When diffusing through the cytoplasm, the intracellular structures such as mitochondria and endoplasmic reticulum hinder the diffusion rate. The diffusion rate within the cytoplasm is approximately 25% that of in free solution (22). Thus, the cytoplasm permeability coefficient is

$$P_{cyt} = \frac{0.25 D_0}{h_{RPE}}. \quad (13)$$

The lateral diffusion pathway is modeled similarly to Edwards & Prausnitz (12). However, in the present model the pathway is divided into two components, one consisting of the free diffusion in the membrane and the other of the diffusion across the TJs. These two parts are connected in series, as solute partitions into the membrane at the basolateral membrane and diffuses freely until the restricting TJs which hinder the diffusion more, similarly to the paracellular pathway. The permeability of both the free and TJ parts is calculated with equation

$$P_{lat,i} = \frac{\varepsilon_{lat,i} K_{mem} D_{lat}}{d_{lat,i}}, \quad (14)$$

where $\varepsilon_{lat,i}$ is a hindrance factor describing the reduction in diffusion rate due to the membrane proteins, K_{mem} is the membrane distribution coefficient, D_{lat} is the lateral diffusion coefficient within the membrane, $d_{lat,i}$ is the diffusion distance and the subscript i is either f or TJ. By assuming that the TJs form a similar barrier against membrane diffusion as with paracellular pathway, it is reasonable to assume that parameter $\varepsilon_{lat,TJ}$ equals α_{leak}. The relation between K_{mem} and K_D was determined by Mitragotri (23) to be

$$K_{mem} = K_D^{0.7}. \quad (15)$$

Mitragotri (23) also modeled the diffusion within lipid bilayer and derived equation

$$D_{lat} = 2 \times 10^{-9} \exp\left[-0.46\left(\frac{r_s}{1.62}\right)^2\right], \quad (16)$$

where r_s has the unit of Å. The division of r_s by 1.62 is added to the equation in the present model to account for the different methods the molecular radius is calculated. This is based on the validation and good fit of the Mitragotri's model with measured values (23). Edwards & Prausnitz (12) calculated the total diffusion distance for a cylindrical cell and it can be adapted for RPE as

$$d_{mem,total} = \tau_{RPE} h_{RPE} + \frac{1}{3} r^*_{RPE}, \quad (17)$$

where r^*_{RPE} is the average radius of the hexagonal RPE cell, which is given as 1.05 r_{RPE}, with r_{RPE} being the center-to-flat cell radius. The lateral TJ diffusion distance is equal to h_{TJ} and the lateral free diffusion distance is calculated as $d_{mem,f} = d_{mem,total} - h_{TJ}$.

The total transcellular permeability is given as

$$P_{trans} = P_{tr} + P_{lat} = \left(\frac{2}{P_{mem}} + \frac{1}{P_{cyt}}\right)^{-1} + \left(\frac{1}{P_{lat,TJ}} + \frac{1}{P_{lat,free}}\right)^{-1}, \quad (18)$$

and the total RPE permeability is calculated as shown in Eq. 1.

Diffusion Across the Bruch's Membrane

A model known as fiber matrix model (12) is used for the BrM model, because it describes interactions between the diffusing solute and stationary fibers. The model is constructed in two scales, including larger collagen fibrils and smaller proteoglycan molecules. Both scales and both layers are modeled as randomly oriented fiber matrices.

Effective diffusion coefficient in a fiber matrix is given by equation

$$D_{eff,m} = \Phi_m D_m, \quad (19)$$

where Φ_m is the matrix partition coefficient and D_m is the diffusion coefficient within the matrix (24). The subscript m denotes collagen or proteoglycan matrix in either the ICL or OCL. A common form for Φ_m in randomly oriented fiber matrices was derived by Ogston (25) as

$$\Phi_m = \exp(-f), \quad (20)$$

where

$$f = \phi_f \left(1 + \frac{r_s}{r_f}\right)^2, \quad (21)$$

and ϕ_f is the fiber volume fraction and r_f is the fiber radius (m).

The diffusion coefficient within the matrix includes the hydrodynamic and steric interactions between the fibers and the solute. These two interactions can be separated into separate factors as shown in equation

$$D_m = F_m S_m D_0, \quad (22)$$

where F_m denotes the hydrodynamic and S_m the steric interactions (26). There are several approaches to calculate each of these factors. For hydrodynamic interactions, a form introduced by Clague & Phillips (27) is used in the present model and is given as

$$F_m = \exp\left(-a\phi_f^b\right), \quad (23)$$

where a and b are fitted parameters that depend on r_s and r_f. A fit proposed by Amsden (28) is used with parameter values $a = \pi$ and $b = 0.174 \ln(59.6\, r_f/r_s)$. Steric interactions are modeled with a commonly used equation derived by Johansson & Löfroth (19):

$$S_m = \exp\left(-0.84 f^{1.09}\right). \quad (24)$$

To define the effective diffusion coefficients within the ICL or OCL, first the effective proteoglycan matrix diffusion coefficients are calculated. This is followed by the calculation of the effective collagen matrix diffusion coefficients, while using

the effective proteoglycan matrix diffusion coefficients instead of D_0 as the base diffusion coefficient in Eq. 22. The BrM permeability coefficient is calculated with equation

$$P_{BrM} = \left(\frac{1}{P_{ICL}} + \frac{1}{P_{OCL}}\right)^{-1} = \left(\frac{d_{ICL}}{D_{ICL}} + \frac{d_{OCL}}{D_{OCL}}\right)^{-1}, \quad (25)$$

where d_{ICL} and d_{OCL} are the ICL and OCL thicknesses (m), respectively. The diffusion coefficient within each layer equals to the corresponding effective collagen matrix diffusion coefficient.

Diffusion Across the Choriocapillaris Endothelium

The diaphragms of the CE fenestrations span over the fenestration leaving triangular openings between the fibers. These openings are modeled with circular openings which fit inside these sectors, as presented in Fig. 2d. Because of the circular openings, the fenestrations can be modeled using the pore model already used for the TJ pores (Eq. 5). The relative surface area of the pores is the product of the relative surface area of the attenuated region, the fenestrations in an attenuated region and the diaphragm pores in a fenestration.

Properties of the Solute Molecules

The molecular properties needed to predict the permeability are free diffusion coefficient, molecular size and lipophilicity. Free diffusion coefficient can be calculated from empirical relationship between the molecular mass and diffusion coefficient derived by Avdeef (29) at 37°C as

$$D_0 = 9.9 \times 10^{-9} M_s^{-0.453}. \quad (26)$$

This equation was fitted using 147 molecules with molecular mass ranging between 30–1,200 Da and with $R^2 = 0.94$ (29).

A commonly used expression relating diffusion coefficient to molecular radius is Stokes-Einstein equation, which does not work for molecules with a radius of under five times that of the solvents. Due to this, a form of this equation derived by Sutherland (30) is used instead, and it is given as

$$r_s = \frac{k_B T}{4\pi\eta D_0}, \quad (27)$$

where k_B is Boltzmann constant (1.38×10^{-23} J K^{-1}), T is the absolute temperature (K), η is the solvents dynamic viscosity (Pa s). This equation assumes that the solvent molecules can slip past the surface of the solute molecules, contrary to Stokes-Einstein equation. Also, Sutherland equation corresponds well to the average of maximum and minimum molecular projection radii calculated with Marvin Calculator Plugins (MarvinSketch 5.10.1, 2012, ChemAxon, http://www.chemaxon.com) (data not shown). A normal body temperature of 310 K and dynamic viscosity of 0.00069 Pa s are used. The model is mainly limited to molecules with molecular mass of under 1,000 Da. The lipophilicity is represented with distribution coefficients at pH 7.4 and the values are calculated with Marvin Calculator Plugins.

Parameter Values

Parameters for RPE

All the parameter values are shown in Table I. The parameters needed for the RPE are the RPE cell and lateral space dimensions, the parameters defining TJs as well as the membrane diffusion hindrance factors. The values of TJ strand height and pore separation are defined by the 10-nm particle structure (14). The TJ region height was measured from images of porcine RPE (32).

The TJ pore radius of 0.44 nm measured by Watson *et al.* (36) was determined by calculating the Stokes-Einstein radius of the PEG oligomer that barely made it through the TJ pores. By combining the data measured by Watson *et al.* and the hindrance factor used in our model, the TJ pore radius is calculated to be 0.48 nm. This radius is transformed first into a molecular mass with the method used by Watson, and then a radius comparable to the solutes in this model is calculated with Eqs. 26 and 27. The value of the TJ leak parameter is approximated based on the results by Watson *et al.* (36) from Caco-2 cells and the magnitude scale of the measured choroid-RPE permeabilities discussed later. Also, the approximated value of α_{leak} is close to the calculated value for renal tubules (15). The free membrane diffusion hindrance factor is assumed to be the same as for the lipid molecules.

Parameter for BrM

The parameters needed for the modeling of the BrM are the ICL and OCL thicknesses, as well as the radii and fiber volume fractions of the proteoglycan and collagen fibrils in both the ICL and OCL. The ICL and OCL thicknesses are calculated from the total BrM thickness of 3 μm (2) and the relative thicknesses of the two layers. The proteoglycans are approximated only by the glycosaminoglycan side chains, neglecting the core proteins. Thus the proteoglycan radius is equal to the glycosaminoglycan radius.

There are no data about the fiber volume fractions in the literature, so they were approximated. The collagen volume fraction in the corneal stroma determined from figures in Ref. (37) is approximately 0.27. Based on the differences in images from the corneal stroma (37) and BrM (16), the values for the BrM are estimated to be higher than those of corneal stroma. Parameters $\phi_{PG,ICL}$ and $\phi_{PG,OCL}$ are the volume fractions when collagen fibrils are ignored, as they only describe the proteoglycan ground substance (11).

Table I The Model Parameter Values

Description	Parameter	Value	Reference
Parameters of the RPE			
RPE cell flat-to-flat diameter	d_{RPE}	10 μm	(31)
RPE cell height	h_{RPE}	12 μm	(31)
Lateral space half-width	W_{LS}	20 nm	(31)
Lateral space tortuosity	τ_{RPE}	1.1	(31)
TJ region height	h_{TJ}	0.4 μm	(32)
TJ strand height	h_{TJs}	10 nm	(14)
TJ strand number	n_{TJs}	4	(33)
TJ pore radius	r_{TJp}	0.82 nm	See text
TJ pore separation	d_{TJp}	10 nm	(14)
TJ leak parameter	α_{leak}	0.0005	See text
Free membrane hindrance factor	$\varepsilon_{lat,f}$	0.42	(34)
Parameters for the BrM			
ICL thickness	d_{ICL}	2 μm	See text
OCL thickness	d_{OCL}	1 μm	See text
Proteoglycan radius	r_{PG}	0.5 nm	(35)
Collagen fibril radius	r_{CF}	30 nm	(4)
Proteoglycan volume fraction in ICL	$\phi_{PG,ICL}$	0.07	See text
Proteoglycan volume fraction in OCL	$\phi_{PG,OCL}$	0.04	See text
Collagen volume fraction in ICL	$\phi_{CF,ICL}$	0.40	See text
Collagen volume fraction in OCL	$\phi_{CF,OCL}$	0.30	See text
Parameters for the CE			
Fenestration height	h_{fen}	20 nm	(32)
Diaphragm pore radius	r_{dia}	3.3 nm	See text
Relative surface area of the diaphragm pores	ε_{dia}	0.0075	See text

Parameters for CE

The fenestration height, diaphragm pore size and relative surface are of the diaphragm pores are the parameters required for the CE. The diaphragm pore radius is calculated by using the sector angle of 45° and sector radius of 12 nm (38). Federman (39) measured the relative attenuated region area to be 0.60. The surface area of the fenestrations inside the regions is calculated from figures in Ref. (38), resulting in value of 0.25. The relative area of the eight diaphragm pores in a fenestration is calculated by assuming the fenestration radius of 40 nm (38), giving a value of 0.05.

Calculations and Experimental Permeability Data Review

The functionality of the BRB model is evaluated by calculating how the permeability of BRB and its components behave as a function of the solute radius and lipophilicity. Value ranges of r_s=5–9 Å (corresponding to M_s=163–598 Da) and log K_D=−3…3 are used, as most of the drug molecules for which there are data fit within these limits.

A sensitivity analysis is conducted to study the importance of certain model parameters by increasing and decreasing the value of these parameters one at a time by 25% and calculating the absolute change in the permeability of the respective BRB component. The parameters chosen for the RPE are n_{TJs}, r_{TJp}, d_{TJp}, α_{leak} and $\varepsilon_{mem,f}$. The first four parameters largely define the TJ model and parameters α_{leak} and $\varepsilon_{mem,f}$ dictate the permeability of the transcellular pathway. The chosen parameters affect both the paracellular and transcellular pathways, so four solutes with different sizes and lipophilicities are used (r_s=6 and 8 nm and log K_D=−2 and 2) to estimate the effect on permeability. For the BrM, parameters $\phi_{PG,ICL}$, $\phi_{PG,OCL}$, $\phi_{CF,ICL}$ and $\phi_{CF,OCL}$ are chosen, because the fiber volume fractions are the uncertain values in the BrM model. As only the solute size affects diffusion in the BrM, two sizes of solutes are used (r_s=6 and 8 nm).

A literature review of the available experimental permeability data from BRB and its components is carried out to compare the measured and experimental results from excised animal eyes. Because of the differences in study methods and tissue sources, only studies with multiple solute molecules are included to show the behavior of the permeability. Furthermore, only molecules with the molecular mass of under 1,000 Da are included. Also, if there are multiple values within a study measured *e.g.* with different concentrations or permeation directions, the coefficient most fitting for passive steady-state diffusion is chosen fitting into our model principles. *E.g.* if there are permeability coefficients for both diffusion directions, the smaller is chosen as the larger value may include the effects of active transport (5). Most permeability studies include choroid, so choroid-RPE system is considered to correspond to BRB and choroid-BrM to BrM. The behavior of choroid-RPE permeability is analyzed only as a function of lipophilicity and, for choroid-BrM permeability, only molecular radius is used. The molecular radius and lipophilicity for the solutes are calculated as described.

RESULTS

Model Behavior

RPE, BrM and CE Models

The behavior of the RPE transcellular (P_{trans}) and paracellular permeabilities (P_{para}) as a function of solute molecular radius and lipophilicity are presented in Fig. 3a and b, respectively. In Fig. 3a, P_{para} decreases logarithmically as the radius increases, but begins to even out with high radii. With all the shown values of log K_D, P_{trans} decreases exponentially with the increasing radius. The change in P_{trans} ranges over four orders of magnitude within the given radius range, compared to the less than one magnitude change in P_{para}. The behaviors of the P_{trans} curves as a function of the radius are similar. As shown in Fig. 3b, lipophilicity has no effect on P_{para}. All three curves for

P_{trans} with different radii increase exponentially over four orders of magnitude within the shown lipophilicity range. The transcellular pathway becomes more significant than the paracellular pathway at log $K_D \geq 0$ for small molecules (r_s <6 Å) and, as the lipophilicity increases, it becomes significant also for medium sized molecules (r_s=6–8 Å). For large solutes (r_s>8 Å), the paracellular pathway is the main diffusion pathway independent of lipophilicity within the given value range.

The behavior of BrM (P_{BrM}) and CE permeabilities (P_{CE}) as a function of the solute radius is shown in Fig. 3c. Both P_{BrM} and P_{CE} decrease exponentially as the radius increases. This decrease is, however, slower than the modeled decrease with transcellular permeability, being less than one order of magnitude within the given range of the increasing radius for both P_{BrM} and P_{CE}.

The BRB components are from the tightest to the leakiest: RPE, BrM and CE. RPE is 600 to 3,000 times less permeable than BrM for solutes with log K_D=0. For very hydrophilic solutes (log K_D=−3) the difference is similar, but for very lipophilic (log K_D=3) and small solutes, the difference is only around 2.7-fold. Also for the given radius range, BrM is on average 4.5 times less permeable than CE.

BRB Model

The rate-limiting components for the total BRB permeability in respect to the molecular properties are depicted in Fig. 3d. The paracellular pathway of the RPE is the dominating component for most solutes, as the transcellular pathway mainly sets the permeability for small and lipophilic solutes. The behavior of the total BRB permeabilities as a function of

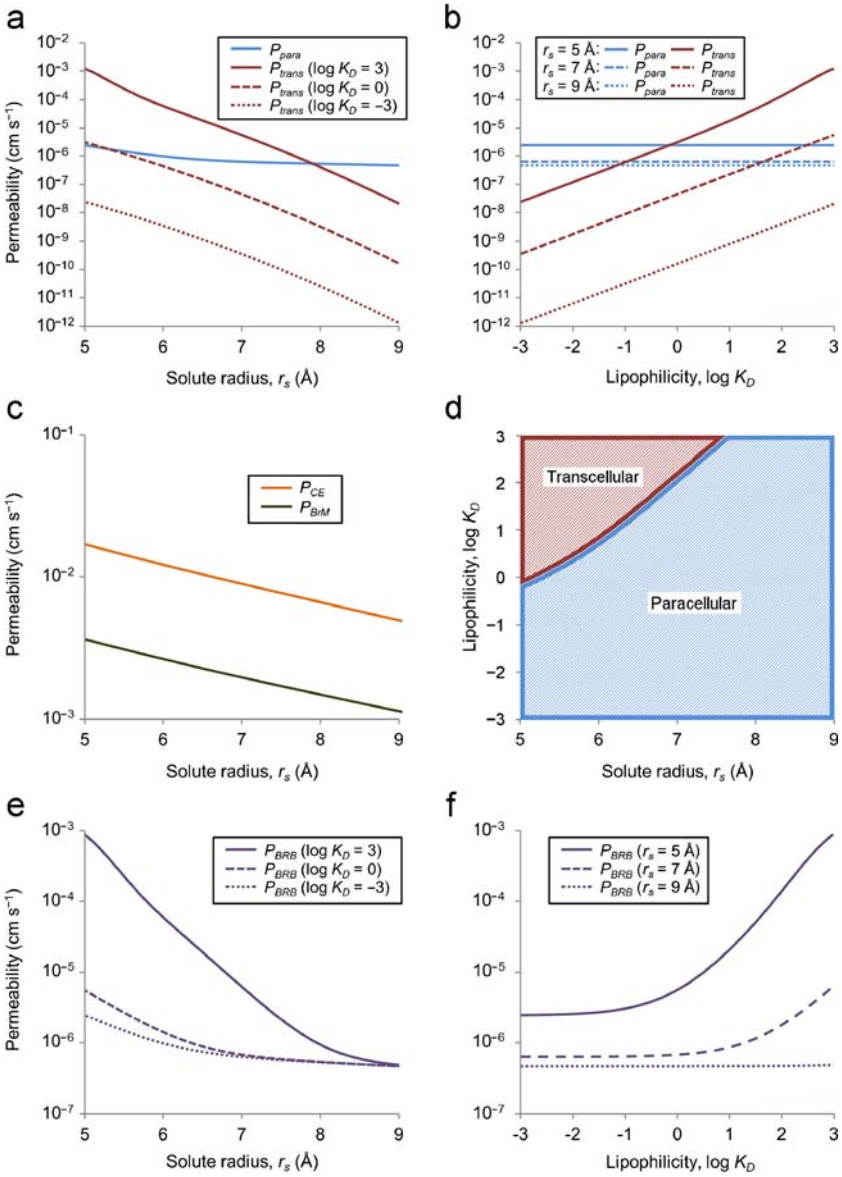

Fig. 3 Results of the model behavior. (**a**) Paracellular (P_{para}) and transcellular permeabilities (P_{trans}) with three lipophilicities as a function solute radius, (**b**) paracellular and transcellular permeabilities with three radii as a function solute lipophilicity, (**c**) Bruch's membrane (P_{BrM}) and choriocapillaris endothelium permeabilities (P_{CE}) as a function of solute radius, (**d**) the rate-limiting pathway of BRB permeability as a function of solute radius and lipophilicity, and total BRB permeability (P_{BRB}) as a function of (**e**) solute radius with three lipophilicities and (**f**) lipophilicity with three radii.

solute radius and lipophilicity is shown in Fig. 3e and f, respectively. For hydrophilic solutes, the radius is the main rate-determining property, but with lipophilic solutes both the radius and lipophilicity are important. The differences in permeability caused by the solute properties become more prominent with small and lipophilic molecules.

Sensitivity Analysis

For RPE, the chosen parameters for the sensitivity analysis were the TJ strand number (n_{TJs}), TJ pore radius (r_{TJp}), TJ pore separation (d_{TJp}), leak parameter (α_{leak}) and free membrane hindrance factor ($\varepsilon_{mem,f}$). The results of this analysis are shown in Fig. 4a. The effect of r_{TJp} on RPE permeability is significant, especially when increasing its value and with small molecules (r_s=6 Å). For small hydrophilic solutes the increase of r_{TJp} by 25%, leads to 2.3-fold change in the RPE permeability (P_{RPE}). The changes of α_{leak} values to both direction lead to around 18–25% change in P_{RPE} for all the solutes, the impact being smaller with small solutes. The effects of both n_{TJs} and d_{TJp} on P_{RPE} are the largest but not significant with small hydrophilic solutes. Finally, there are no notable effects caused by the changes in $\varepsilon_{mem,f}$.

For BrM, the parameters for sensitivity analysis included the proteoglycan and collagen volume fractions in the ICL and OCL ($\phi_{PG,ICL}$, $\phi_{PG,OCL}$, $\phi_{CF,ICL}$ and $\phi_{CF,OCL}$). The results are shown in Fig. 4b. The ICL volume fractions, *i.e.* $\phi_{PG,ICL}$ and $\phi_{CF,ICL}$, appear to be the most significant, as changes in them lead to respective changes of 15–23% and 35–47% in BrM permeability (P_{BrM}). The difference between the two sizes of solutes (r_s=6 and 8 Å) is generally small, excluding $\phi_{PG,ICL}$ for which there is 4–6% difference. The changes in both the OCL volume fractions are insignificant.

Review of Experimental Permeability Data

The literature review revealed that the available experimental permeability data is insufficient for the validation of the BRB model. With the given preconditions, 48 independent permeability values were found for choroid-RPE tissue and 23 for choroid-BrM. The choroid-RPE values are from bovine (5,40), porcine (40,41) and rabbit (40) with a lipophilicity range of −2.12…2.79, and those of choroid-BrM from bovine (42), porcine (42,43) and human (44) with a radius range of 3.51–8.10 Å (corresponding to M_s=75–474 Da). The measured choroid-RPE permeability coefficients as a function of lipophilicity presented so far in the literature are shown in Fig. 5a, excluding the rabbit data as it has similar behavior as the other species in that study (40) and thus does not provide new information. Permeability data of choroid-BrM as a function of molecular radius in presented in Fig. 5b.

As can be seen, there is no clear behavior in the choroid-RPE permeability results as a whole. Two of the studies concluded that the permeability increases as the lipophilicity increases (5,41) while the third one (40) concluded the opposite. There is no systematic difference between the animals. For choroid-BrM, the permeability decreases as a function of the molecular size. However, between two studies (42,43), there are differences of over three orders of magnitude in choroid-BrM permeability for large molecules.

When comparing the results of our model (Fig. 3f) and the measured permeability values (Fig. 5a) for the whole BRB, there is no clear agreement of the behavior as a function of lipophilicity but the magnitudes between the two are in similar scale. Between the predicted and measured values for the BrM, there is a difference of at least one order of magnitude depending on which of the two experimental studies is used and the behavior is similar.

DISCUSSION

We constructed a model of passive diffusion across the outer blood-retinal barrier (BRB). To our best knowledge, this is the first model for BRB that is based on the physicochemical properties of both the BRB and the diffusing solute molecule, defining the interactions between the two during diffusion. This makes the model suitable for the studies of drug permeation through the BRB, for molecule-specific pharmacokinetic models as well as to help construct *in vitro* BRB models.

The model consists of the three-layered structure of the BRB—the retinal pigment epithelium (RPE), Bruch's membrane (BrM) and choriocapillaris endothelium (CE). Although the model is created to represent *in vivo* systemic drug administration, suitable model components can be utilized as needed for other models, such as those for transscleral delivery routes. This three-layer structure is more accurate representation of the BRB than any of the preceding models that include passive diffusion across the BRB. In addition, compared with the corneal model (12) used as a framework for our model, the TJ model and treatment of molecular properties presented here are more detailed in structure.

Our TJ model represents the static biological TJ structure (14) fairly accurately. However, the TJ are a dynamic structure with many factors regulating their function. For example, the physical interactions between the RPE cells and the retinal photoreceptors, chemical secreted factor, pharmacological methods as well as ions like potassium can regulate the permeability of the tight junctions (33,45). In addition to the regulatory factors, the accuracy of our static TJ model could be further enhanced by including the web-like strand structure. Furthermore, including the TJ pore charge selectivity and non-uniform pore sizes and spacing (14) could improve the model but would simultaneously make it more complex.

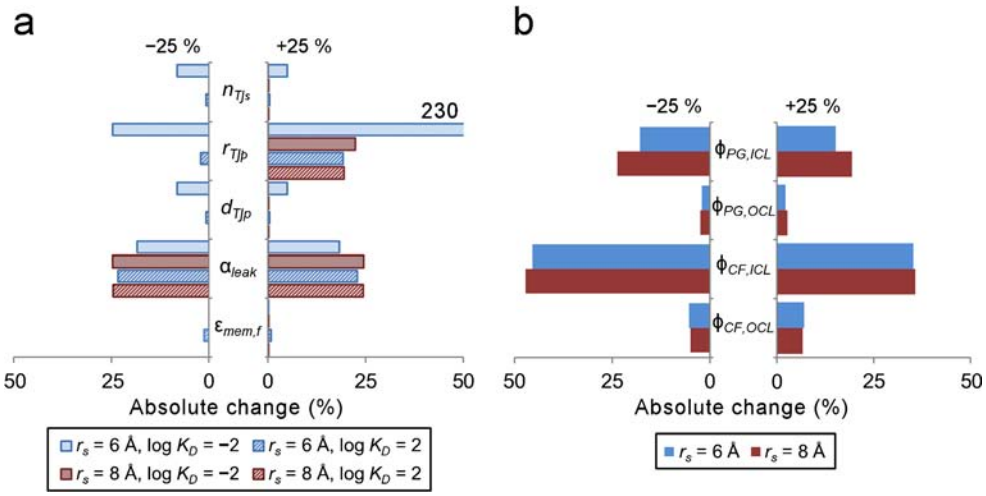

Fig. 4 Results of the sensitivity analysis, showing the absolute changes on (**a**) P_{RPE} and (**b**) P_{BrM} when parameter values are changed ± 25%. The parameters for the RPE: n_{TJs} TJ strand number, r_{TJp} TJ pore radius, d_{TJp} TJ pore separation, α_{leak} leak parameter, $\varepsilon_{mem,f}$ free membrane hindrance factor, and for the BrM : proteoglycan and collagen volume fractions in the ICL and OCL, $\phi_{PG,ICL}$, $\phi_{PG,OCL}$, $\phi_{CF,ICL}$ and $\phi_{CF,OCL}$.

Model Behavior

The present work investigates the permeability behavior of BRB and its parts in relation to the solute radius and lipophilicity. RPE is divided into paracellular and transcellular pathways, which are structurally very different. In the transcellular pathway, the diffusion of the solute depends on the diffusion of the lipids (13), whereas in the paracellular pathway a route for permeation already exists. Furthermore, the independence of the paracellular pathway of the solute's lipophilicity makes it a general rate-limiting pathway for the solute permeation, because the transcellular permeability decreases rapidly with the decreasing lipophilicity.

When examining the transcellular pathway in more detail, it is notable that that the transverse transcellular pathway is insignificant in comparison with the lateral diffusion transcellular pathway. For instance, for a solute with log K_D=2 and r_s=6 Å, the lateral diffusion pathway is around 50 times more permeable than the transverse pathway. One reason for this may be that the solutes lipophilic enough to partition into a cell membrane tend to remain inside it rather than partition into the aqueous cytosol. The difference between the transverse and lateral diffusion pathways was also noted by Edwards & Prausnitz (12) in their corneal model, and they reasoned it to result from the data used to derive the cell membrane permeation model. The main difference in permeability behavior between our model and the corneal model (12) is that in our model the lateral diffusion pathway depends on the solute size. This can be seen with large solutes (r_s=9 Å) as the permeability does not depend on lipophilicity in our model, unlike in the corneal model with the corresponding solutes (12).

According to our model, the effect of BrM or CE on the total BRB permeability is small due to their higher permeabilities. The simplification of only including the fenestrations in the CE model was justified, as its permeability exceeds both those of RPE and BrM and thus has no effect on the total BRB permeability.

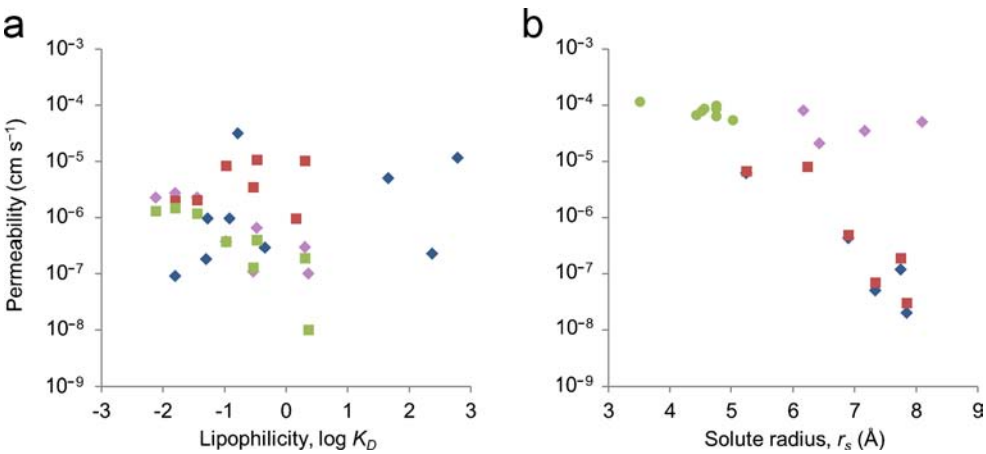

Fig. 5 Results for the permeability literature review. (**a**) Choroid-RPE permeability as a function of lipophilicity in porcine (*blue diamonds* (41) and *purple diamonds* (40)) and bovine eyes (*red squares* (5) and *green squares* (40)) and (**b**) choroid-BrM permeability as a function of solute radius in porcine (*blue diamonds* (42) and *purple diamonds* (43)), bovine (*red squares* (42)) and human eyes (*green dots* (44)).

Model Parameters

The sensitivity and importance of certain parameters from both the RPE and BrM models was studied by changing their value by 25% to both directions and calculating the change in the permeability of the respective component. According to our results in the paracellular TJ pathway, the most important parameter is the TJ pore radius (r_{TJp}), which defines the solute size limit for the TJ pore pathway. On the other hand, the uniform changes in permeability of all the four solutes caused by changes in the leak parameter (α_{leak}) indicate that it sets the magnitude for the whole RPE permeability. As the paracellular pathway is generally the rate-limiting one, it is obvious that r_{TJp} and α_{leak} together define the RPE permeability. Neither of these parameters was used in the model by Edwards & Prausnitz (12). Based on the sensitivity analysis on their corneal model, they found the parameters of the lateral diffusion pathway—lateral diffusion coefficient and pathway length—to be the most important parameters for corneal epithelium (12). This indicates relative unimportance of the TJs in their model compared to ours.

With BrM, the main interest is in the approximated proteoglycan and collagen fibril volume fractions. The volume fractions in the ICL ($\phi_{PG,ICL}$ and $\phi_{CF,ICL}$) are significantly more important than those in the OCL ($\phi_{PG,OCL}$ and $\phi_{CF,OCL}$), because of their larger values as well as the difference of thicknesses between the two BrM layers. Furthermore, due to the large amount of collagen, its effects are larger in both layers. The differences between solute sizes are generally miniscule. For collagen this results from the large size difference between the solutes ($r_s < 1$ nm) and fibrils ($r_{CF} = 30$ nm). The solute size difference is more noticeable with $\phi_{PG,ICL}$, because of the similar radius of the solutes and proteoglycans. Edwards & Prausnitz (12) also found that the volume fractions mostly define the permeability of the corneal stroma.

The RPE permeability dominates the total BRB permeability in our model. Therefore it is clear that they are both largely defined by two parameters: the TJ pore radius and the leak parameter. Their importance reflects the mutual significance of both the paracellular and lateral diffusion pathways, as already seen with the model behavior. There was not much data to base the approximations of the important parameters, mainly the leak parameter and the collagen volume fraction in the ICL. As the leak parameter largely defines the magnitude of the total BRB permeability in our model and magnitude is similar between the predictions and the experimental results, it seems the approximation was good. In a very recent study (46), the packing density of collagen fibrils in the ICL, which can be thought to correspond to $\phi_{CF,ICL}$, was calculated to be 0.48. Our approximation ($\phi_{CF,ICL} = 0.40$) is relatively close. The sensitivity analysis shows, that the corresponding 20% increase of $\phi_{CF,ICL}$ is not enough to make the BrM permeability a significant component in the whole BRB permeability.

Available Experimental BRB Permeability Data

Unfortunately very limited number of studies has been conducted to obtain experimental data of BRB permeability. There are only three studies providing the permeability coefficients of the entire BRB (5,40,41). Steuer *et al.* (41) used only one measurement time point (30 min) to calculate the permeability, which may cause issues due to the longer lag times of lipophilic molecules compared with the hydrophilic ones to reach equilibrium (5). Further, there was conflicting results. The reason for the conflict in behavior between the results by Pitkänen *et al.* (5) and Kadam *et al.* (40) may be that the latter calculated the choroid-RPE permeability by subtracting the permeability of the sclera from the permeability of the sclera-choroid-RPE. This may affect the comparability of the permeabilities of solutes with different lipophilicities due to tissue binding in sclera. Moreover, Pitkänen *et al.* (5) measured only the permeability of the choroid-RPE and because of this, the behavior measured by them can be considered more suitable in relation to the present model. However, it is noteworthy that the magnitudes of the permeabilities of the hydrophilic molecules are similar between Pitkänen *et al.* (5) and Kadam *et al.* (40), which indicates that the conflict in behavior is more prominent with lipophilic solutes. Pitkänen *et al.* (5) also measured the effect of molecular size on the BRB permeability and showed that the permeability decreases as molecular size increases. Their test molecules were beyond the size limit of the present model, but they indicate similar behavior. Furthermore, a factor that may affect the comparability of the experimental permeability results are the regulatory mechanisms that affect the TJ permeability discussed earlier. Due to the very limited amount of the experimental work in the literature, it is practically impossible to validate our BRB model with the available data. However, we can conclude that the model produces permeability coefficients with similar magnitudes and behavior as a function of the molecular properties in comparison with the experimental measurements.

The challenge in measuring the BrM permeability is that it is a very thin tissue layer and thus difficult to extract intact. Thus, all the experimental studies include the choroid in the measurement sample (42–44). Based on the literature review, the BrM permeability decreases as a function of molecular size, but the absolute values for just the BrM permeability are unknown because of the choroid. The magnitude difference between the permeability results by Cheruvu & Kompella (42) and Pescina *et al.* (43) might be a consequence of the higher solute concentration used by the latter, because high concentrations saturate the tissue with the bound solutes and thus lead to higher permeabilities. Anyhow, our model predicts a permeability coefficient of at least one magnitude higher than the measured permeability values, which may indicate the effect of the choroid on the measured values as well as an

issue in the model. This issue may arise from the unsuitability of the fiber matrix model for the BrM, the approximations of the unknown parameter values or the simplifications done in the model.

For 4 kDa FITC-dextrans, there is around 70 to 170-fold difference between the permeabilities across choroid-RPE and choroid-BrM (5). For small molecules, the difference between the two depends on what experimental results are compared. For example, if the values by Kadam *et al.* (40) and Cheruvu & Kompella (42)—measured with similar setups—are compared, there is no significant difference between them. This may point out a large effect of the choroid and the inaccuracy it causes in the results. Based on the existing data, it is impossible to estimate the real difference between the RPE and BrM permeabilities.

Comparison with Other Models

The present model includes a structurally more detailed description of the BRB than any of the preceding pharmacokinetic models (6–10). Also, when compared with the corneal model by Edwards & Prausnitz (12), which was used as a framework for our model, there are certain biological differences and model improvements. Firstly, the baseline permeability of the corneal endothelium, which is modeled similarly to the RPE as they are both monolayers, is around one order of magnitude higher than that of the RPE. This permeability is set by the paracellular pathway, and the TJs are tighter in the present RPE model, which corresponds well to the difference in the measured permeabilities from the BRB and cornea (5,12). The TJ geometry is completely different between our model and the corneal model (12). The earlier model used only a narrowed slit to represent TJs and our model uses a two-pathway model with more accurate geometry. The TJ structure in our model is similar to the TJ model of the renal tubules by Guo *et al.* (15), but the motive for the models is different: our model tries to predict the permeabilities, whereas the model of the renal tubules studied the structure of the TJs. The other major difference between the corneal model and ours is the significance of molecular size with lipophilic solutes as discussed before.

The phenomenological descriptive model by Haghjou *et al.* (10) related certain molecular properties to the permeability across RPE-choroid-sclera in a rabbit eye by using multiple linear regression. The best fit for hydrophilic molecules (log $K_D<0$) depended on lipophilicity and protein binding. Molecular size was also quite significant factor, but did not contribute to the accuracy of the model. Lipophilicity did not greatly affect the permeability of hydrophilic solutes in the present model, as they generally do not pass any lipophilic barriers. For lipophilic molecules (log $K_D>0$), Haghjou *et al.* (10) did not find a good fit with the permeability data, which may partly explain the variability in the choroid-RPE permeability data discussed earlier and the challenge of modeling the transcellular pathway.

Model Challenges and Limitations

The main challenge in modeling the BRB is the lack of biological experimental data of some of the structural parameters of the BRB and its components. This was compensated by approximating some of their values, such as the leak parameter or the BrM volume fractions, mainly based on data obtained from other tissues. The approximation of some important parameters creates uncertainty in the model. Furthermore, as already discussed, the lack of suitable and consistent permeability data prevents proper validation.

As our model is of passive diffusion only, the specific effects of active transport on the permeability are ignored. Active transport processes are specific for each molecule, and thus not suitable for a model based solely on basic molecular descriptors, and there is very little comprehensive data to model them. Although the experimental data may include active transport processes, which reduce the feasibility of comparison between the model and the experimental results, it is at the moment the closest suitable data for the evaluation of the BRB model's functionality. Likewise, the model does not take into account the solute binding into extra- or intracellular structures, such as the melanin pigment within the RPE cells. Melanin binding is a specific process and has been shown to affect the permeability (40,43). The dynamic binding is difficult to incorporate into a steady-state model, although a method proposed to include the matrix binding (42) could be used here: diffusion constant (D_{cyt}) is divided by $1+K$, where K is an association constant specific for each solute, for which there is no extensive experimental data. In addition, this would have only affected the already-insignificant transverse diffusion pathway and our model represents a steady-state situation, in which time- and concentration-dependent phenomena are neglected. Also, some refinements for our TJ model were discussed earlier.

For BrM, the accuracy and number of the layers and biomolecules could be increased. In addition to proteoglycans and collagen, BrM contains other biomolecules, such as lipids which accumulate from the RPE and affect the permeability (4). However, the lack of data of all the layers and biomolecules prevents further improvements at this time. Furthermore, as shown by Pescina *et al.* (43), permeability across choroid-BrM does depend on lipophilicity because of the specific melanin binding in the tissue. However, the choroid is much thicker than the BrM which most probably affects the results significantly, thus making any approximations of its effect solely on BrM difficult. Electrostatic interactions between the fibers and solutes are ignored as well although they could be incorporated into the model (47).

The main simplification with the solute molecules was the assumed spherical shape. Most molecules are irregularly shaped, so for example the orientation of a molecule trying to diffuse through a TJ pore becomes significant. However, the slit, pore and fiber-matrix models also assume this geometry, and it would need statistical or random Markov type models to take into account the individual shape of each molecule.

CONCLUSIONS

In this study, a computational, structure-based model of passive diffusion across the BRB was constructed generally based on the corneal model by Edwards & Prausnitz (12). Our model shows rather good correspondence in magnitude with the experimental results. Accurate validation, however, is not feasible due to the lack of consistency in the reported experimental data indicating great variation in the permeability behavior between the studies. Our model indicates that the paracellular pathway of the RPE largely defines the permeability of the whole BRB, the transcellular pathway having some effect with small and lipophilic solutes. The parameter sensitivity analysis shows that many of the parameters we were forced to approximate are important and further studies are needed to define more accurate values for many structural properties of the RPE and BRB as a whole. Despite the lack of data, the model presented here is the most accurate model of passive diffusion through BRB and our TJ model is more accurate than those in the other structure-based models for other barriers. The model gathers the knowledge of the BRB permeability. Thus the model presented her can be used as a base for future BRB models utilizing coming experimental data as well as for testing the hypotheses of BRB permeability for drug molecules. Hence, this type of models has a potential to reduce the need of animal experiments as well as save resources.

ACKNOWLEDGMENTS AND DISCLOSURES

The study was financially supported by the Academy of Finland (grant numbers 252225 and 260375) and TEKES—the Finnish Funding Agency for Technology and Innovation (grant number 718/31/2011).

REFERENCES

1. Strauss O. The retinal pigment epithelium in visual function. Physiol Rev. 2005;85(3):845–81.
2. Bhutto I, Lutty G. Understanding age-related macular degeneration (AMD): relationships between the photoreceptor/retinal pigment epithelium/Bruch's membrane/choriocapillaris complex. Mol Aspects Med. 2012;33(4):295–317.
3. Del Amo EM, Urtti A. Current and future ophthalmic drug delivery systems. A shift to the posterior segment. Drug Discov Today. 2008;13(3–4):135–43.
4. Booij JC, Baas DC, Beisekeeva J, Gorgels TGMF, Bergen AAB. The dynamic nature of Bruch's membrane. Prog Retin Eye Res. 2010;29(1):1–18.
5. Pitkänen L, Ranta V-P, Moilanen H, Urtti A. Permeability of retinal pigment epithelium: effects of permeant molecular weight and lipophilicity. Investig Ophthalmol Vis Sci. 2005;46(2):641–6.
6. Mac Gabhann F, Demetriades AM, Deering T, Packer JD, Shah SM, Duh E, *et al.* Protein transport to choroid and retina following periocular injection: theoretical and experimental study. Ann Biomed Eng. 2007;35(4):615–30.
7. Amrite AC, Edelhauser HF, Kompella UB. Modeling of corneal and retinal pharmacokinetics after periocular drug administration. Investig Ophthalmol Vis Sci. 2008;49(1):320–32.
8. Ranta V-P, Mannermaa E, Lummepuro K, Subrizi A, Laukkanen A, Antopolsky M, *et al.* Barrier analysis of periocular drug delivery to the posterior segment. J Control Release. 2010;148(1):42–8.
9. Balachandran RK, Barocas VH. Computer modeling of drug delivery to the posterior eye: effect of active transport and loss to choroidal blood flow. Pharm Res. 2008;25(11):2685–96.
10. Haghjou N, Abdekhodaie MJ, Cheng Y-L. Retina-choroid-sclera permeability for ophthalmic drugs in the vitreous to blood direction: quantitative assessment. Pharm Res. 2013;30(1):41–59.
11. Edwards A, Prausnitz MR. Fiber matrix model of sclera and corneal stroma for drug delivery to the eye. AIChE J. 1998;44(1):214–25.
12. Edwards A, Prausnitz MR. Predicted permeability of the cornea to topical drugs. Pharm Res. 2001;18(11):1497–508.
13. Mitragotri S. Modeling skin permeability to hydrophilic and hydrophobic solutes based on four permeation pathways. J Control Release. 2003;86(1):69–92.
14. Anderson JM, Van Itallie CM. Physiology and function of the tight junction. Cold Spring Harb Perspect Biol. 2009;1(2):1–16.
15. Guo P, Weinstein AM, Weinbaum S. A dual-pathway ultrastructural model for the tight junction of rat proximal tubule epithelium. Am J Physiol Ren Physiol. 2003;285(2):F241–57.
16. Goldbaum MH, Madden K. A new perspective on Bruch's membrane and the retinal pigment epithelium. Br J Ophthalmol. 1982;66(1):17–25.
17. Bearer EL, Orci L. Endothelial fenestral diaphragms: a quick-freeze, deep-etch study. J Cell Biol. 1985;100(2):418–28.
18. Ho NFH, Raub TJ, Burton PS, Barsuhn CL, Audus KL, Borchardt RT. Quantitative approaches to delineate passive transport mechanisms in cell culture monolayers. In: Amidon GL, Lee PI, Topp EM, editors. Transport processes in pharmaceutical systems. New York: Marcel Dekker, Inc; 2000. p. 219–316.
19. Johansson L, Löfroth J-E. Diffusion and interaction in gels and solutions. 4. Hard sphere Brownian dynamics simulations. J Chem Phys. 1993;98(9):7471–9.
20. Dechadilok P, Deen WM. Hindrance factors for diffusion and convection in pores. Ind Eng Chem Res. 2006;45(21):6953–9.
21. Lieb WR, Stein WD. Non-Stokesian nature of transverse diffusion within human red cell membranes. J Membr Biol. 1986;92(2):111–9.
22. Verkman AS. Solute and macromolecule diffusion in cellular aqueous compartments. Trends Biochem Sci. 2002;27(1):27–33.
23. Mitragotri S. A theoretical analysis of permeation of small hydrophobic solutes across the stratum corneum based on Scaled Particle Theory. J Pharm Sci. 2002;91(3):744–52.
24. Johnson EM, Berk DA, Jain RK, Deen WM. Diffusion and partitioning of proteins in charged agarose gels. Biophys J. 1995;68(4):1561–8. Elsevier.
25. Ogston AG. The spaces in a uniform random suspension of fibres. Trans Faraday Soc. 1958;54(1):1754–7.
26. Phillips RJ. A hydrodynamic model for hindered diffusion of proteins and micelles in hydrogels. Biophys J. 2000;79(6):3350–3.

27. Clague DS, Phillips RJ. Hindered diffusion of spherical macromolecules through dilute fibrous media. Phys Fluids. 1996;8(7):1720–31.
28. Amsden B. Solute diffusion within hydrogels. Mechanisms and Models. Macromolecules. 1998;31(23):8382–95.
29. Avdeef A. Leakiness and size exclusion of paracellular channels in cultured epithelial cell monolayers-interlaboratory comparison. Pharm Res. 2010;27(3):480–9.
30. Sutherland WLXXV. A dynamical theory of diffusion for non-electrolytes and the molecular mass of albumin. Philos Mag. 1905;9(54):781–5.
31. Garron LK. The ultrastructure of the retinal pigment epithelium with observations on the choriocapillaris and Bruch's membrane. Trans Am Ophthalmol Soc. 1963;61:545–88.
32. Prünte C, Kain HL. Enzymatic digestion increases permeability of the outer blood-retinal barrier for high-molecular-weight substances. Graefes Arch Clin Exp Ophthalmol. 1995;233(2):101–11.
33. Rajasekaran SA, Hu J, Gopal J, Gallemore R, Ryazantsev S, Bok D, *et al.* Na, K-ATPase inhibition alters tight junction structure and permeability in human retinal pigment epithelial cells. Am J Physiol Cell Physiol. 2003;284(6):C1497–507.
34. O'Leary TJ. Lateral diffusion of lipids in complex biological membranes. Proc Natl Acad Sci U S A. 1987;84(2):429–33.
35. Ogston AG, Preston BN, Wells JD. On the transport of compact particles through solutions of chain-polymers. Proc R Soc A Math Phys Eng Sci. 1973;333(1594):297–316.
36. Watson CJ, Rowland M, Warhurst G. Functional modeling of tight junctions in intestinal cell monolayers using polyethylene glycol oligomers. Am J Physiol Cell Physiol. 2001;281(2):C388–97.
37. Hirsch M, Prenant G, Renard G. Three-dimensional supramolecular organization of the extracellular matrix in human and rabbit corneal stroma, as revealed by ultrarapid-freezing and deep-etching methods. Exp Eye Res. 2001;72(2):123–35.
38. Melamed S, Ben-Sira I, Ben-Shaul Y. Ultrastructure of fenestrations in endothelial choriocapillaries of the rabbit—a freeze-fracturing study. Br J Ophthalmol. 1980;64(7):537–43.
39. Federman JL. The fenestrations of the choriocapillaris in the presence of choroidal melanoma. Trans Am Ophthalmol Soc. 1982;80:498–516.
40. Kadam RS, Cheruvu NPS, Edelhauser HF, Kompella UB. Sclera-choroid-RPE transport of eight β-blockers in human, bovine, porcine, rabbit, and rat models. Investig Ophthalmol Vis Sci. 2011;52(8):5387–99.
41. Steuer H, Jaworski A, Elger B, Kaussmann M, Keldenich J, Schneider H, *et al.* Functional characterization and comparison of the outer blood-retina barrier and the blood–brain barrier. Investig Ophthalmol Vis Sci. 2005;46(3):1047–53.
42. Cheruvu NPS, Kompella UB. Bovine and porcine transscleral solute transport: influence of lipophilicity and the Choroid-Bruch's layer. Investig Ophthalmol Vis Sci. 2006;47(10):4513–22.
43. Pescina S, Santi P, Ferrari G, Padula C, Cavallini P, Govoni P, *et al.* Ex vivo models to evaluate the role of ocular melanin in trans-scleral drug delivery. Eur J Pharm Sci. 2012;46(5):475–83.
44. Hussain A, Rowe L, Marshall J. Age-related alterations in the diffusional transport of amino acids across the human Bruch's-choroid complex. J Opt Soc Am A. 2002;19(1):166.
45. Peng S, Rahner C, Rizzolo LJ. Apical and basal regulation of the permeability of the retinal pigment epithelium. Investig Ophthalmol Vis Sci. 2003;44(2):808–17.
46. Warnke PH, Alamein M, Skabo S, Stephens S, Bourke R, Heiner P, *et al.* Primordium of an artificial Bruch's membrane made of nanofibers for engineering of retinal pigment epithelium cell monolayers. Acta Biomater. 2013. doi:10.1016/j.actbio.2013.07.029.
47. Johnson EM, Deen WM. Electrostatic effects on the equilibrium partitioning of spherical colloids in random fibrous media. J Colloid Interface Sci. 1996;178(2):749–56.